

Hybrid quantum device with a carbon nanotube and a flux qubit for dissipative quantum engineering

Xin Wang,^{1,2} Adam Miranowicz,^{2,3,*} Hong-Rong Li,^{1,†} and Franco Nori^{2,4,‡}

¹Institute of Quantum Optics and Quantum Information, School of Science, Xi'an Jiaotong University, Xi'an 710049, China

²CEMS, RIKEN, Wako-shi, Saitama 351-0198, Japan

³Faculty of Physics, Adam Mickiewicz University, 61-614 Poznań, Poland

⁴Physics Department, The University of Michigan, Ann Arbor, Michigan 48109-1040, USA

(Received 19 December 2016; revised manuscript received 24 April 2017; published 12 May 2017)

We describe a hybrid quantum system composed of a micrometer-sized carbon nanotube (CNT) longitudinally coupled to a flux qubit. We demonstrate the usefulness of this device for generating high-fidelity nonclassical states of the CNT via dissipative quantum engineering. Sideband cooling of the CNT to its ground state and generating a squeezed ground state, as a mechanical analog of the optical squeezed vacuum, are two additional examples of the dissipative quantum engineering studied here. Moreover, we show how to generate a long-lived macroscopically distinct superposition (i.e., a Schrödinger-cat-like) state. This cat state can be trapped, under some conditions, in a dark state, as can be verified by detecting the optical response of control fields.

DOI: 10.1103/PhysRevB.95.205415

I. INTRODUCTION

The quantum engineering of nanomechanical systems, which enables the generation of nonclassical states of their mechanical motion, has a variety of applications, such as exploring the classical-quantum boundary [1,2], high-precision metrology [3–5], and quantum information processing [6]. It has been discussed extensively in hybrid platforms, such as optomechanical and electromechanical systems [7–10]. However, mechanical oscillators dissipate energy when exposed to a noisy environment at finite temperature [11,12], and it is still challenging to generate their nonclassical states with high purity. To overcome this problem, *dissipative engineering of long-lived nonclassical states of mechanical motions* has been studied extensively (see, e.g., Refs. [13–15] and references therein). This is the subject of this paper.

Recently, mechanical resonators made of carbon nanotubes (CNTs) [16–25] have attracted considerable attention due to their distinctive advantages. These include high-frequency oscillations [17–19], small mass, and a high-quality factor up to several millions [17,20]. Since CNTs have a large current-carrying capacity [23–25], it is possible to couple them with superconducting quantum circuits [26–32] to form quantum electromechanical systems. Recent experiments [33–35] have discussed how to combine these two systems together, e.g., to couple quantum dots in CNTs with a superconducting quantum interference device (SQUID) and resonators. The novel stamping technologies fabricating these two isolated artificial systems together are rather mature [34]. However, to couple the motion of a CNT with SQUIDs, one needs to fabricate such a CNT into the SQUID loop and might require strong external magnetic fields [36].

Even though the coherence time of a CNT can be much longer than that of a qubit, it is difficult to manipulate or detect the quantum coherence of phonons in a CNT for two

reasons: First, the position displacement of a CNT is too tiny to be detected effectively under current experimental techniques, and the energy of a phonon is much weaker than that of a photon [7,10,37]. Second, it is difficult to create the strong coupling between phonons and other systems (for example, detectors).

In this paper, we propose strongly coupled hybrid systems, where a current-carrying CNT interacts with a flux qubit via longitudinal coupling. In this setup, the CNT is suspended separately above the qubit loop, rather than being fabricated into the circuits. The decoherence noise can be minimized by operating the flux qubit at its optimal point and placing the CNT at a special symmetric position. Based on this platform, we show that it is possible to employ this strong longitudinal coupling for dissipative engineering of the CNT via the rapid decay of the qubit. Examples include cooling to its ground and squeezed states, and trapping the mechanical motion into long-lived macroscopically distinct superpositions with a high fidelity. Moreover, without adding other setups, we demonstrate that it should be possible to check for imperfections in the trapped dark Schrödinger cat states by detecting the optical response of the control fields. Therefore, it is possible to manipulate and observe quantum features of phonons based on our proposal.

II. MODEL

We consider a setup as shown in Fig. 1(a), in which a gap-tunable superconducting flux qubit [38–42] is coupled to a current-carrying CNT [16–18]. The flux qubit is of an eight-shaped gradiometric topology, which allows the independent control of the magnetic energy bias ϵ and the gap Δ [38,39]. The model Hamiltonian for the qubit is

$$H = \frac{1}{2}(\Delta\sigma_z + \epsilon\sigma_x), \quad (1)$$

where $\sigma_z = |e\rangle\langle e| - |g\rangle\langle g|$, and $\sigma_x = \sigma_+ + \sigma_- = |e\rangle\langle g| + |g\rangle\langle e|$ are the Pauli operators in the qubit basis, $|e\rangle$ and $|g\rangle$. For brevity, hereafter we set $\hbar = 1$. Moreover, $\epsilon = 2I_p(\Phi_q - \Phi_0/2)$, with the flux Φ_q through the qubit and the flux quantum Φ_0 , and persistent current I_p (see, e.g., Refs. [41,42]). The

* miran@amu.edu.pl

† hrli@mail.xjtu.edu.cn

‡ fnori@riken.jp

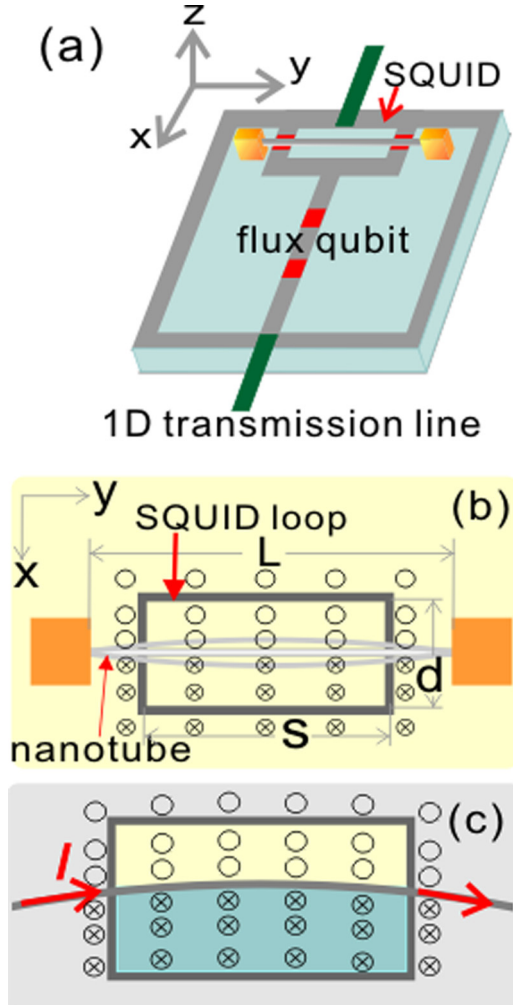


FIG. 1. Schematic diagrams of the flux qubit hybrid system with a carbon nanotube (CNT). (a) An eight-shaped flux qubit is placed on the x - y plane with a current-carrying CNT suspended above its SQUID. The red bars represent the Josephson junctions. The green line is the central conductor of the 1D transmission line stretched in two directions. (b) Specifically: a CNT of length L is located at the central position along the SQUID (of length S and width d). (c) The dc current I , which flows through the CNT (displaced from its equilibrium position), produces a flux in the SQUID. The qubit and CNT are coupled via the motion-induced-flux imbalance between the up (yellow) and down (blue) sections.

energy gap Δ is controlled by the flux f_s through the SQUID (of length S and width d), and it is expressed as

$$\Delta = \Delta(f_{s0}) + R(\delta f_s), \quad (2)$$

where f_{s0} is the static flux though the SQUID, $R = \partial\Delta(f_s)/(\partial f_s)$ is the flux sensitivity of the energy gap [43,44], and δf_s describes the flux perturbations due to external control fields.

As shown in Fig. 1, the CNT is suspended above the SQUID in the central-symmetric position and interacts with the SQUID via the magnetic field produced by its dc current I . We assume that the CNT is longer than the SQUID length, and it can be approximately viewed as a long current line. At its equilibrium position, $x = 0$, the flux contribution of the current I through

the SQUID loop is zero. However, when the CNT starts to vibrate around $x = 0$, the extra flux perturbation due to the area imbalance can be expressed as $\delta f_s = \mu_0 I L \Delta x / (\pi d)$. Thus, the displacement of the CNT,

$$\Delta x = \frac{1}{\sqrt{2m\omega_m}}(a + a^\dagger), \quad (3)$$

gives rise to a linear modulation of the energy gap of the qubit, where m (ω_m) is the effective mass (frequency) of the CNT. Since the CNT is placed symmetrically on the qubit, the flux contribution from the current I on the energy bias ϵ vanishes to first order [43,44], i.e., the vibration mode decouples from the qubit loop. Moreover, to minimize the pure dephasing effect, we assume that the flux qubit is operated at its degeneracy point with $\epsilon = 0$ (see, e.g., Refs. [43,44]). We consider driving currents through a 1D transmission line [45] [the green line in Fig. 1(a)], which produce magnetic fields of opposite signs in the two-qubit loops [46]. Therefore, the currents interact with the qubit via the dipole matrix element $\mu = \langle e | M I_p \sigma_x | g \rangle$, where M is the mutual inductance. Moreover, the transmission line is placed symmetrically perpendicular to the CNT, so their mutual inductance can be zero. Thus, the CNT and the transmission line do not interact with each other. Assuming that the ac drive current amplitude I_i has frequency ω_i , the drive strength is $2\epsilon_i = \mu I_i$. The total Hamiltonian becomes

$$H = \frac{\omega_q}{2}\sigma_z + \omega_m a^\dagger a + g\sigma_z(a^\dagger + a) + \sum_i 2\epsilon_i \sigma_x \cos(\omega_i t), \quad (4)$$

where $\omega_q = \Delta(f_{s0})$ is the qubit frequency, and

$$g = \frac{R\mu_0 I L}{\pi d \sqrt{2m\omega_m}} \quad (5)$$

is the qubit-phonon coupling strength. Different from the Rabi model in standard QED systems, a longitudinal coupling between the qubit and the CNT is induced [47–49]. Note that the Hamiltonian, given in Eq. (4), is not at all specific to the hybrid structure based on the CNT, but only the numbers discussed in the following paragraphs are specific. For example, analogous couplings occur in both circuit-QED [49] and trapped-ion [50] systems. Thus, the study presented here has a much wider applicability.

We consider that the CNT oscillates at a frequency $\omega_m/(2\pi) = 50$ MHz, length $5 \mu\text{m}$, and mass $m = 4 \times 10^{-21} \text{ kg}$ (see, e.g., Refs. [17–21,51]), and it carries a dc current $I = 50 \mu\text{A}$ (see, e.g., Refs. [23–25]). For the qubit, the length and width of the SQUID loop can be about 3 and $0.6 \mu\text{m}$, respectively, and the flux sensitivity of the energy gap [41,43] can reach $R = 0.7 \text{ GHz}/(m\Phi_0)$. Using these parameters, we obtain the coupling strength $g/(2\pi) = 3.4 \text{ MHz}$, i.e., the Lamb-Dicke parameter $\lambda = g/\omega_m \simeq 0.07$. In experiments, the flux sensitivity R and dc current I can be adjusted by changing the gap position $\Delta(f_{s0})$ and the voltage applied to the CNT gate, respectively. Therefore, the coupling strength g can be tuned conveniently.

In realistic situations, we should consider all the decoherence channels. For a CNT, the quality factor of the vibration mode can be $\sim 5 \times 10^6$ (see, e.g., Ref. [20]). The dephasing rate of the qubit can be effectively suppressed by operating at its degeneracy point $\epsilon = 0$. Here we employ the decay channel

of the qubit to drive the CNT into nonclassical states, and the decay rate of a flux qubit around ~ 0.5 MHz is achievable in experiments [42,52]. The mechanical motion of the CNT might couple to a thermal reservoir with finite temperature T , and the corresponding thermal phonon number is $n_{\text{th}} = [\exp(\omega_m/k_B T) - 1]^{-1}$. We assume that the hybrid system is weakly coupled to a large environment with extremely short environmental-memory time, and the Born-Markov approximation is valid here. The dynamics of this hybrid system can be described by the Lindblad master equation

$$\frac{d\rho(t)}{dt} = -i[H, \rho(t)] + \Gamma D[\sigma_-]\rho(t) + n_{\text{th}}\gamma D[a^\dagger]\rho(t) + (n_{\text{th}} + 1)\gamma D[a]\rho(t), \quad (6)$$

where $\rho(t)$ is the time-dependent density matrix of the hybrid system, and $D[o]\rho = (1/2)(2o\rho o^\dagger - o^\dagger o\rho - \rho o^\dagger o)$ is the Lindblad superoperator. Assuming that this hybrid system has a temperature $T \sim 15$ mK, the thermal phonon number is about $n_{\text{th}} \approx 5$. Thus, the coupling is much stronger than the decoherence of the vibration mode, i.e., $g \gg n_{\text{th}}\gamma$.

It should be stressed that the current fluctuation $\delta I(t) (\ll I)$ through the CNT might lead to additional decoherence of the qubit [41]. Moreover, it might be difficult to place the CNT at the exact central position of the SQUID. Thus, the two areas might be slightly imbalanced due to the fabricating imperfection. Similar to the discussions in Refs. [41,43], the current noise is only sensitive to the area imbalance, rather than to the whole area of the loop. In addition, the effect of the flux noise in the SQUID is much smaller than that for the qubit [41]. Therefore, the decoherence induced by the current fluctuation $\delta I(t)$ can be effectively suppressed via this spatial arrangement.

III. COOLING THE MOTION TO THE GROUND AND SQUEEZED GROUND STATES

Novel ideas about dissipative engineering of a macroscopic motion into squeezed states, by cooling the Bogoliubov mode into the dark state, were proposed in Refs. [53–56] and were recently realized in microwave optomechanical systems [57]. Sideband cooling of a mechanical mode into its ground states can be viewed as a special case of preparing squeezing by assuming that the blue-sideband-drive strength is zero [58–62]. This method creates stationary squeezed and ground states with the assistance of qubit decay channels. Here we will show how these methods are employed in this longitudinal-coupling system. We will show how this method is employed in this longitudinal-coupling system.

As shown in Fig. 2, to drive the mechanical mode into the dark squeezed states, two coherent-drive fields are required, respectively, of blue and red sidebands with strengths ϵ_\pm and frequencies $\omega_\pm = \omega_q \pm \omega_m$. We obtain the effective Hamiltonian as

$$H_{\text{eff,s}} = \Theta\sigma_+B + \text{H.c.}, \quad (7)$$

where $\Theta = 2\lambda\sqrt{\epsilon_- - \epsilon_+}$ is the coupling rate and B is the Bogoliubov mode, defined as

$$B = a^\dagger \sinh \eta + a \cosh \eta, \quad (8)$$

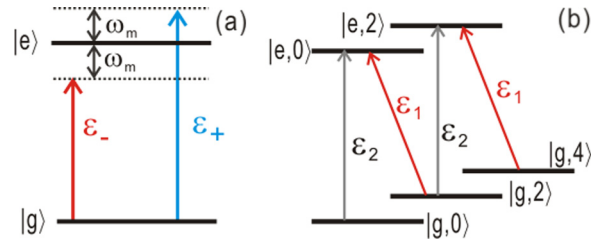


FIG. 2. Schematic diagrams showing how to cool down and engineer the mechanical mode of the CNT into (a) a squeezed state and (b) a macroscopically distinct coherent-state superposition (i.e., a Schrödinger-cat-like state).

with $\tanh \eta = -\epsilon_+/\epsilon_-$. The slow decoherence process of the CNT can be neglected, and the effective Hamiltonian $H_{\text{eff,s}}$, together with the qubit decay terms in Eq. (6), describes the cooling process of the Bogoliubov mode to its ground state [53,54]. It can easily be verified that the unique stationary state of the system is $|\Psi_s\rangle = |\psi_s\rangle|g\rangle$, where

$$|\psi_s\rangle = \exp\left[\frac{1}{2}(\eta a^2 - \eta^* a^{\dagger 2})\right]|0\rangle \quad (9)$$

is the squeezed ground state with squeezing ratio η . This is a mechanical analog of the optical squeezed vacuum. Therefore, we create stationary squeezed states with the assistance of decay channels.

By assuming the only nonzero drive to be the red sideband (i.e., $\epsilon_- > 0$ and $\epsilon_+ = 0$), the CNT can be cooled to its ground state. This effect is similar to the standard sideband cooling in optomechanical and electromechanical systems [58–62]. The steady state for the system is the ground state with no squeezing, and the effective cooling Hamiltonian reduces to the standard Jaynes-Cummings model under the rotating-wave approximation:

$$H_{\text{eff,s}} = g_c\sigma_+a + \text{H.c.}, \quad (10)$$

with $g_c = 2\lambda\epsilon_-$. Assuming $\Gamma \gg g_c$, the excited state of the qubit can be eliminated adiabatically. The stationary average phonon number satisfies [56] $\bar{n} = (n_{\text{th}}\gamma\Gamma)/(2g_c^2)$. Since the cooperativity of the system $C = g_c^2/\gamma\Gamma \gg 1$ is extremely high, the ground state can be achieved easily with $\bar{n} \sim 10^{-3}$ under current experimental parameters.

IV. CAT-STATE GENERATION

Due to rapid decoherence of the mechanical motion, it is still challenging to observe and coherently manipulate macroscopically distinct superpositions (i.e., Schrödinger-cat-like states) in realistic systems [15,63–71]. To overcome the decoherence problem, dissipative engineering of a mechanical resonator into conditional steady superposition states has been discussed [14,72,73] for quadratic-coupling optomechanical systems. However, the boson-boson quadratic coupling is too weak to create observable Schrödinger-cat-like states under current experimental approaches [72–75]. Here we show a way to produce a long-lived Schrödinger-cat-like state by employing an induced strong quadratic spin-phonon coupling.

As shown in Fig. 2(b), we applied bichromatic drives for the qubit: a red-sideband drive with detuning $\approx 2\omega_m$, and a

resonant drive with strengths (frequencies) $\epsilon_1(\omega_1)$ and $\epsilon_2(\omega_2)$, respectively.

By applying the unitary transformation $U_1 = \exp[-\lambda\sigma_z(a^\dagger - a)]$ to the total Hamiltonian in Eq. (4), we obtain

$$H = \frac{1}{2}\omega_q\sigma_z + \omega_m a^\dagger a + \sum_{i=1,2} \epsilon_i [\sigma_+ e^{-i\omega_i t} e^{2\lambda(a^\dagger - a)} + \text{H.c.}] \quad (11)$$

Here we assume that ϵ_1 is a strong off-resonant drive strength inducing sideband transitions, and it is much stronger than ϵ_2 . To obtain a quadratic coupling, we expand H , in the small parameter λ , to second and zeroth orders for the terms ϵ_1 and ϵ_2 , respectively, and we perform the unitary transformation $U = \exp(-i\omega_1\sigma_z t)$. Thus, we obtain

$$\begin{aligned} H = & \frac{1}{2}\Delta\sigma_z + \omega_m a^\dagger a + \epsilon_1(\sigma_+ + \sigma_-) \\ & + 2\epsilon_1[\lambda\sigma_+(a^\dagger - a) + \lambda^2\sigma_+(a^\dagger - a)^2 + \text{H.c.}] \\ & + [\epsilon_2\sigma_+e^{-i\delta_{12}t} + \text{H.c.}], \end{aligned} \quad (12)$$

where $\Delta = \omega_q - \omega_1 \simeq 2\omega_m$ is the detuning between the qubit and sideband drives, and $\delta_{12} = \omega_2 - \omega_1$ is the detuning between the two drives. The third term induces the dynamical Stark shift of the qubit. Moreover, due to the coupling and sideband transition, the frequency of the CNT will also be slightly renormalized. The shifted frequencies for the qubit and CNT can be expressed as [76]

$$\tilde{\Delta} = \sqrt{\Delta^2 + 4\Omega_p^2}, \quad \omega'_m = \omega_m - \frac{4\epsilon_1^2 g^2}{3\omega_0^3}. \quad (13)$$

We consider the resonant case $\tilde{\Delta} = 2\omega'_m = \delta_{12}$. Performing the unitary transformation $U = \exp[-i(\tilde{\Delta}\sigma_z/2 + \omega'_m a^\dagger a)t]$, and neglecting all the rapidly oscillating terms, the Hamiltonian reduces to

$$H_{\text{eff,c}} = 2\epsilon_1\lambda^2(\sigma_+a^2 + \sigma_-a^{\dagger 2}) + \epsilon_2(\sigma_+ + \sigma_-), \quad (14)$$

where the first term describes the two-phonon sideband transitions. We can rewrite this effective Hamiltonian as

$$H_{\text{eff,c}} = (\Theta_c\sigma_+a^2 + \epsilon_2\sigma_+) + \text{H.c.} \quad (15)$$

by denoting $\Theta_c = 2\lambda^2\epsilon_1$, which is the effective two-phonon transition rate. The spin-boson interaction in Eq. (15) is analogous to the purely bosonic coupling in Refs. [72,73], where the qubit operator is replaced by those of the cavity field. Since the decoherence of the high-quality-factor CNT is extremely slow, we only consider the unitary Hamiltonian in Eq. (15) and the qubit rapid-decay terms in Eq. (6), and the dark state for this dissipative system is $|\Psi_c\rangle = |\psi_c\rangle|g\rangle$, where $|\psi_c\rangle$ should satisfy the equation $(\Theta_c a^2 + \epsilon_2)|\psi_c\rangle = 0$ (see Ref. [77]). If the CNT is initially in an even (odd) Fock state (e.g., $|0\rangle$ and $|1\rangle$), the steady states are also even (odd) coherent states (i.e., the famous bosonic prototypes of Schrödinger-cat-like states), which are

$$|\psi_{\alpha,\pm}\rangle = N^{-1/2}(|\alpha\rangle \pm |-\alpha\rangle), \quad (16)$$

with coherent states $|\pm\alpha\rangle$ ($\alpha = \sqrt{-\epsilon_2/\Theta_c}$), and $|\psi_{\alpha,+}\rangle$ ($|\psi_{\alpha,-}\rangle$) is the even (odd) coherent states with $N = 2[1 + \exp(-2|\alpha|^2)]$. We consider the cooling method, which was described in Sec. III, to initially prepare the system into its

ground state $|0\rangle$. After that, the cooling field is shut down and bichromatic drives are applied. The dark state $|\psi_{\alpha,+}\rangle$ will be successfully trapped. We define the fidelity of this target state as $F = \langle\psi_{\alpha,+}|\rho_m|\psi_{\alpha,+}\rangle$, where ρ_m is the reduced density matrix of the mechanical mode. Moreover, we use the Wigner function,

$$W(\alpha) = \pi^{-2} \int d^2\beta e^{\alpha\beta^* - \alpha^*\beta} \text{Tr}(e^{\beta a^\dagger - \beta^* a} \rho_m), \quad (17)$$

to reveal some nonclassical quantum features of the mechanical states [78]. Specifically, we apply the nonclassical volume of Ref. [79], which is defined as the doubled-integrated negative volume of the Wigner function,

$$\delta_N = \int |W(\alpha)| d^2\alpha - 1, \quad (18)$$

to describe how the superposition interference effects are different from classical behavior: Higher nonclassical volumes δ_N indicate more apparent nonclassical features.

Figure 3(a) shows the evolution of the fidelity F of the target superposition states. Without mechanical decay ($\gamma = 0$), the fidelity F gradually increases and reaches its highest value ~ 0.96 , indicating that the mechanical mode is asymptotically driven into the superposition state $|\psi_{\sqrt{2},+}\rangle$. The highest fidelity cannot be 1 due to the high-order terms induced by the off-resonant drive ϵ_1 , which are eliminated when deriving the effective Hamiltonian $H_{\text{eff,c}}$ (see Ref. [77]). However, with an extremely slow rate, they would still lead to an even-odd sideband transition, i.e., $|g\rangle|2n\rangle \longleftrightarrow |e\rangle|2n \pm 1\rangle$. Moreover, by assuming $n_{\text{th}} = 5$ and $\gamma = 10$ Hz, the thermal noise will also induce a transition from even to odd Fock states and vice versa. Compared with the nondecaying case, the fidelity decreases faster, and $F_{\text{max}} \simeq 0.93$ (at $t_{\text{max}} \simeq 27$ μ s, the dashed line). However, since γ is extremely slow, the superposition features can last for a long time.

Moreover, the time evolution of the nonclassical volume δ_N is plotted in Fig. 3(a) and in its inset (with a much longer time scale). The nonclassical volume first reaches its maximum value $\delta_{N,\text{max}}$, and then starts to decrease due to the thermal noise and the deterioration from the oscillating terms. However, the strength of these processes is extremely low compared with the preparation rate, and the evolution time $\delta_N > 0$ is very long (~ 1 ms), which might be enough to detect various nonclassical features of the states.

In Fig. 3(b), we plotted the highest fidelity $F_{\text{t,max}}$ and the maximum negative volume $\delta_{N,\text{max}}$ versus the resonant drive strength ϵ_1 (i.e., corresponding to the amplitude α of coherent states $|\pm\alpha\rangle$) with constant quadratic strength Θ_c . As seen from the plot, $\delta_{N,\text{max}}$ increases with ϵ_1 indicating that this nonclassical signature of the superposition states becomes more apparent. This is because, with increasing amplitude α , the coherent states $|\alpha\rangle$ and $|-\alpha\rangle$ become nearly orthogonal, and, thus, more separable and distinct. The *quantum superposition* features are now more evident. However, with continually increasing α , the preparation process needs a much longer time, during which thermal noise can destroy the target states. As a result, the fidelity $F_{\text{t,max}}$ decreases with increasing ϵ_1 . When $\epsilon_1/(2\pi) \geq 0.1$ MHz, both $F_{\text{t,max}}$ and $\delta_{N,\text{max}}$ start to decrease due to these processes. Of course, by reducing the effects of the thermal environment (by using

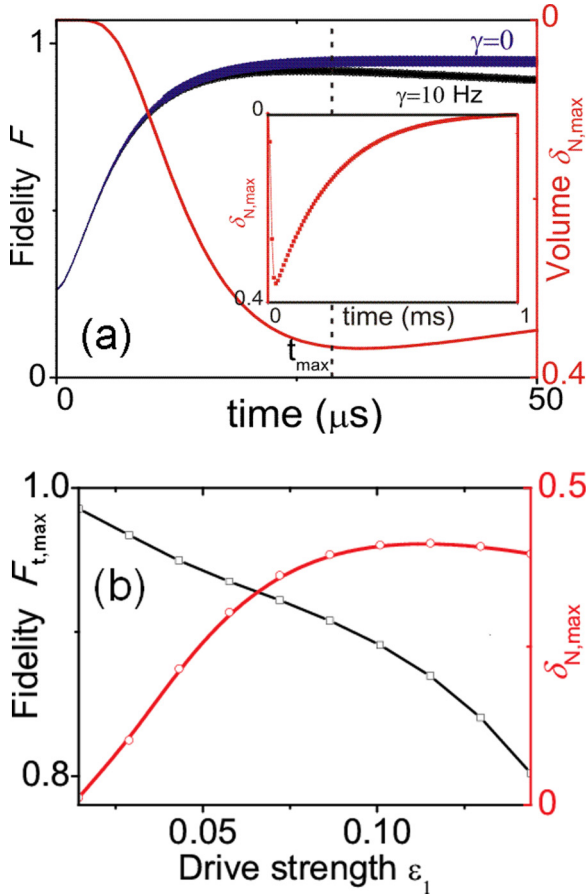


FIG. 3. (a) Time evolutions of the target-state fidelity F for the mechanical decaying and nondecaying cases, and the nonclassical volume δ_N . The inset shows the evolution of δ_N in a much longer time scale. (b) The maximum fidelity $F_{t,\max}$ and the nonclassicality volume $\delta_{N,\max}$ vs the resonant driving strength ϵ_1 . The vertical dashed line in (a) indicates $t_{\max} = 27.5 \mu\text{s}$ corresponding to the maximum of F . In panel (a) we assume $\epsilon_1/(2\pi) = 5 \text{ MHz}$ and $\lambda = 0.06$, corresponding to the quadratic coupling strength $\Theta_c/(2\pi) = 2\lambda^2\epsilon_1 = 36 \text{ KHz}$. The other parameters are $\Gamma/(2\pi) = 0.4 \text{ MHz}$, $n_{\text{th}} = 5$, $\gamma/(2\pi) = 10 \text{ Hz}$, and $\epsilon_2/(2\pi) = -72 \text{ KHz}$.

a CNT with a higher quality factor or working at lower temperatures), we can choose a larger ϵ_2 to generate more distinct Schrödinger-cat-like states.

In Fig. 4(a), we plotted the phonon-number Fock distribution for the Schrödinger-cat-like state generated at time t_{\max} , which is marked by the dashed line in the inset of Fig. 3(a). This clearly shows that only the even Fock states are effectively occupied, while the odd ones have very low amplitudes. Figure 4(b) shows the corresponding Wigner function. We observe two obvious negative regimes and interference-based evidence for the cat states.

V. DETECTING DARK-STATE TRAPPING

Once the whole system is trapped into the dark superposition states, the sideband and resonant transitions have equal amplitudes but opposite signs, leading to destructive interference, which is similar to the coherent population process in Λ -type atomic systems [80]. After the dark state is trapped,

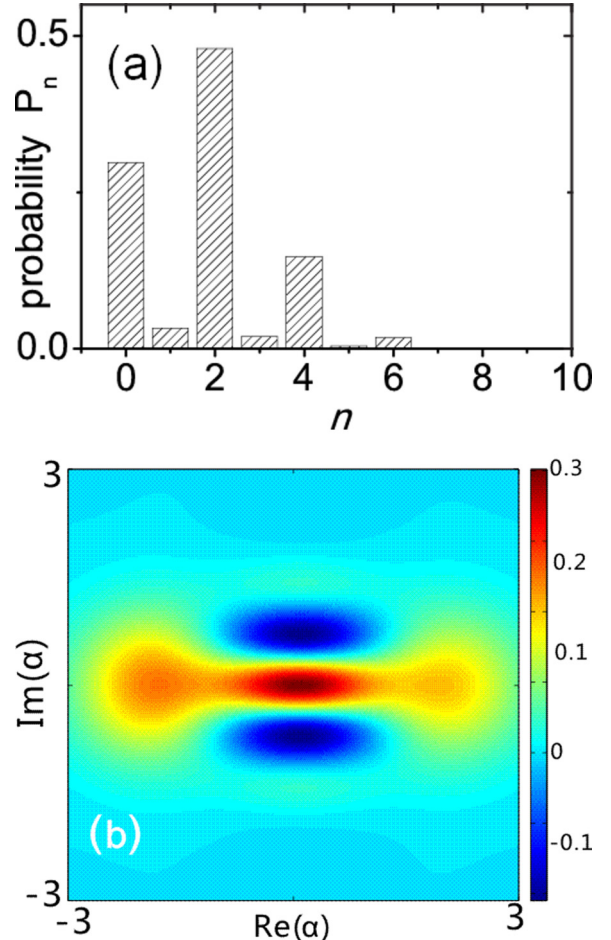


FIG. 4. (a) The phonon-number (Fock-state) distribution and (b) the Wigner function $W(\alpha)$ for the Schrödinger-cat-like state generated at the evolution time $t_{\max} = 27.5 \mu\text{s}$ [indicated by the vertical dashed line in Fig. 3(a)] corresponding to the maximum of the fidelity F . Other parameters are the same as in Fig. 3(a).

we can observe electromagnetically induced transparency (EIT) [81–85]. Without adding any other auxiliary detecting setups, one can measure the reflected control fields to confirm the preparation of the dark states [86–88]. For the resonant-frequency component ω_2 , the scattered current amplitude can be expressed as $I_{\text{sc}} = i\Gamma\langle\sigma_+\rangle/\mu$, and the reflection coefficient is defined as [45]

$$r(\omega_2) = -\frac{I_{\text{sc}}}{I_2} = \frac{i\Gamma\langle\sigma_+\rangle}{(2\epsilon_2)}, \quad (19)$$

for which real and imaginary parts are related to reflection and dispersion, respectively. In experiments, the quadratic coupling might be off-resonantly induced with detuning Δ_d . In Fig. 5(a), we fix the resonant drive parameters, and we show how the highest fidelity F_{\max} and the reflection rate r change with the sideband detuning Δ_d . It is clearly seen that, at the resonant sideband detuning $\Delta_d = 0$, there is almost no reflection for the resonant drive with $\text{Re}(r) = \text{Im}(r) \simeq 0$, and F_{\max} reaches its maximum. When Δ_d starts to bias from zero, F_{\max} starts to decrease, and both $\text{Im}(r)$ and $|\text{Re}(r)|$ increase rapidly, indicating that the resonant drive field is strongly reflected by the flux qubit. It can be found that a Lorentzian dip

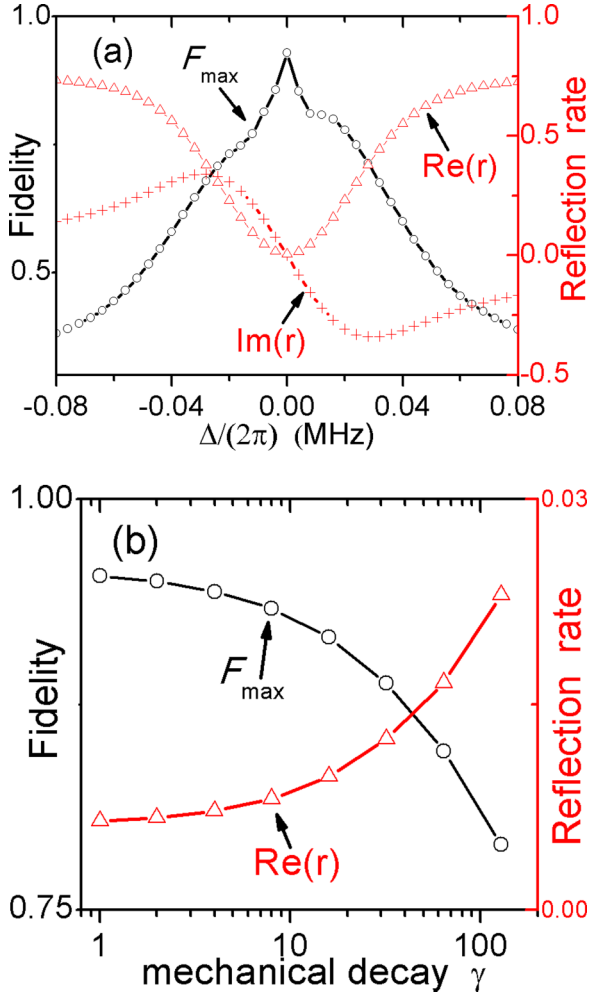


FIG. 5. (a) The highest fidelity F_{max} , dispersion rate $Im(r)$, and reflection rate $Re(r)$, vs (a) the detuning Δ_d and (b) the mechanical decay rate γ . In (b), since $Im(r) \ll Re(r)$, $Im(r)$ is not shown. Other parameters are the same as those in Fig. 3.

occurs in $Re(r)$, while $Im(r)$ follows a typical EIT dispersion curve around $\Delta_d = 0$.

In Fig. 5(b), by considering the resonant case of $\Delta_d = 0$ [corresponding to the dip in $Re(r)$ in Fig. 5(a)], we plot $Re(r)$ and F_{max} versus the CNT decay rate γ . [$Im(r)$ is not shown, since $Im(r) \ll Re(r)$.] It can be clearly found that, when increasing γ , the highest fidelity F_{max} decreases rapidly, and the reflection coefficient $Re(r)$ also increases. Unfortunately, the reflection coefficient is not sensitive as in the detuning case. Specifically, when $\gamma = 130$ Hz, the highest fidelity is $F_{max} \simeq 0.80$, while the reflection coefficient is only $Re(r) \simeq 0.024$, which is too weak to be effectively measured in experiments. This is because the dark state depends on the initial states and is not unique, and the rapid mechanical decay

results in the fidelity decreasing quickly, while only a large γ has a significant effect on the dip of the reflection rate [77,88]. Thus, the error transitions caused by the thermal noise cannot be observed with a high sensitivity from the optical response of the qubit. However, if we can confirm that the mechanical decay is extremely slow, observing the EIT of the control fields can also be a strong indicator for the dark cat-state generation. A detailed discussion of this method and its applications will be presented elsewhere [77].

VI. CONCLUSIONS

We proposed a hybrid quantum system in which the mechanical motion of a CNT strongly interacts with a flux qubit via a longitudinal coupling. In such a system, the decoherence of the qubit can be effectively suppressed. We showed how the ground and squeezed ground states of the CNT can be achieved by sideband cooling.

Moreover, by inducing a strong quadratic coupling in this hybrid system, we can generate macroscopically distinct superposition states (Schrödinger-cat-like states) of the mechanical mode by taking advantage of the decay of the qubit. Since we consider dark states and a high-quality-factor CNT, the superposition can live a long time. We have shown that these cat states can be trapped in a dark state assuming that the CNT dissipation is negligible compared to the qubit dissipation. However, some experiments might satisfy the opposite condition: the CNT dissipation being larger than the qubit dissipation. Still, the original assumption could be realized, e.g., by adding an extra noise to the qubit, while keeping the CNT dissipation fixed. Finally, we showed how to reveal the trapping of the dark superposition states by observing the optical response of the control fields.

Our proposal can also be employed to demonstrate other nonclassical mechanical effects, such as phonon blockade [76,89,90] or generating macroscopically-distinct superpositions of more than two states (i.e., Schrödinger kitten states) [91,92], and it might also serve as a nanomechanical quantum detector of weak forces or other weak signals.

ACKNOWLEDGMENTS

The authors acknowledge fruitful discussions with D. Hou. X.W. is supported by the China Scholarship Council (Grant No. 201506280142). A.M. and F.N. acknowledge the support of a grant from the John Templeton Foundation. F.N. was partially supported by the RIKEN iTHES Project, MURI Center for Dynamic Magneto-Optics via the AFOSR Award No. FA9550-14-1-0040, the Japan Society for the Promotion of Science (KAKENHI), the IMPACT program of JST, JSPS-RFBR Grant No. 17-52-50023, and CREST Grant No. JPMJCR1676.

-
- [1] A. Bassi and G. Ghirardi, Dynamical reduction models, *Phys. Rep.* **379**, 257 (2003).
 - [2] A. Bassi, K. Lochan, S. Satin, T. P. Singh, and H. Ulbricht, Models of wave-function collapse, underlying theories, and experimental tests, *Rev. Mod. Phys.* **85**, 471 (2013).
 - [3] W. J. Munro, K. Nemoto, G. J. Milburn, and S. L. Braunstein, Weak-force detection with superposed coherent states, *Phys. Rev. A* **66**, 023819 (2002).
 - [4] V. Giovannetti, S. Lloyd, and L. Maccone, Advances in quantum metrology, *Nat. Photon.* **5**, 222 (2011).

- [5] T. J. Volkoff and U. R. Fischer, Amplification of the quantum superposition macroscopicity of a flux qubit by a magnetized Bose gas, *Phys. Rev. A* **94**, 042320 (2016).
- [6] K. Stannigel, P. Komar, S. J. M. Habraken, S. D. Bennett, M. D. Lukin, P. Zoller, and P. Rabl, Optomechanical Quantum Information Processing with Photons and Phonons, *Phys. Rev. Lett.* **109**, 013603 (2012).
- [7] M. Blencowe, Quantum electromechanical systems, *Phys. Rep.* **395**, 159 (2004).
- [8] P. Meystre, A short walk through quantum optomechanics, *Ann. Phys.* **525**, 215 (2012).
- [9] Z. L. Xiang, S. Ashhab, J. Q. You, and F. Nori, Hybrid quantum circuits: Superconducting circuits interacting with other quantum systems, *Rev. Mod. Phys.* **85**, 623 (2013).
- [10] M. Aspelmeyer, T. J. Kippenberg, and F. Marquardt, Cavity optomechanics, *Rev. Mod. Phys.* **86**, 1391 (2014).
- [11] K. C. Schwab and M. L. Roukes, Putting mechanics into quantum mechanics, *Phys. Today* **58**(7), 36 (2005).
- [12] M. Poot and H. S. J. van der Zant, Mechanical systems in the quantum regime, *Phys. Rep.* **511**, 273 (2012).
- [13] D. Porras and J. J. García-Ripoll, Shaping an Itinerant Quantum Field into a Multimode Squeezed Vacuum by Dissipation, *Phys. Rev. Lett.* **108**, 043602 (2012).
- [14] M. J. Everitt, T. P. Spiller, G. J. Milburn, R. D. Wilson, and A. M. Zagoskin, Engineering dissipative channels for realizing Schrödinger cats in SQUIDS, *Front. ICT* **1**, 1 (2014).
- [15] M. Abdi, P. Degenfeld-Schonburg, M. Sameti, C. Navarrete-Benlloch, and M. J. Hartmann, Dissipative Optomechanical Preparation of Macroscopic Quantum Superposition States, *Phys. Rev. Lett.* **116**, 233604 (2016).
- [16] V. Sazonova, Y. Yaish, H. Üstünel, D. Roundy, T. A Arias, and P. L. McEuen, A tunable carbon nanotube electromechanical oscillator, *Nature (London)* **431**, 284 (2004).
- [17] A. K. Hüttel, G. A. Steele, B. Witkamp, M. Poot, L. P. Kouwenhoven, and H. S. J. van der Zant, Carbon nanotubes as ultrahigh quality factor mechanical resonators, *Nano Lett.* **9**, 2547 (2009).
- [18] G. A. Steele, A. K. Hüttel, B. Witkamp, M. Poot, H. B. Meerwaldt, L. P. Kouwenhoven, and H. S. J. van der Zant, Strong coupling between single-electron tunneling and nanomechanical motion, *Science* **325**, 1103 (2009).
- [19] E. A. Laird, F. Pei, W. Tang, G. A. Steele, and L. P. Kouwenhoven, A high quality factor carbon nanotube mechanical resonator at 39 GHz, *Nano Lett.* **12**, 193 (2011).
- [20] J. Moser, A. Eichler, J. Güttinger, M. I. Dykman, and A. Bachtold, Nanotube mechanical resonators with quality factors of up to 5 million, *Nat. Nanotechnol.* **9**, 1007 (2014).
- [21] A. Benyaminini, A. Hamo, S. V. Kusminskiy, F. von Oppen, and S. Ilani, Real-space tailoring of the electron-phonon coupling in ultraclean nanotube mechanical resonators, *Nat. Phys.* **10**, 151 (2014).
- [22] P. Stadler, W. Belzig, and G. Rastelli, Ground-State Cooling of a Carbon Nanomechanical Resonator by Spin-Polarized Current, *Phys. Rev. Lett.* **113**, 047201 (2014).
- [23] Z. Yao, C. L. Kane, and C. Dekker, High-Field Electrical Transport in Single-Wall Carbon Nanotubes, *Phys. Rev. Lett.* **84**, 2941 (2000).
- [24] A. Javey, J. Guo, M. Paulsson, Q. Wang, D. Mann, M. Lundstrom, and H. J. Dai, High-Field Quasiballistic Transport in Short Carbon Nanotubes, *Phys. Rev. Lett.* **92**, 106804 (2004).
- [25] J. Yu, G. X. Liu, A. V. Sumant, V. Goyal, and A. A. Balandin, Graphene-on-diamond devices with increased current-carrying capacity: Carbon sp₂-on-sp₃ technology, *Nano Lett.* **12**, 1603 (2012).
- [26] J. Q. You and F. Nori, Superconducting circuits and quantum information, *Phys. Today* **58**(11), 42 (2005).
- [27] J. Clarke and F. K. Wilhelm, Superconducting quantum bits, *Nature (London)* **453**, 1031 (2008).
- [28] L. DiCarlo, M. D. Reed, L. Sun, B. R. Johnson, J. M. Chow, J. M. Gambetta, L. Frunzio, S. M. Girvin, M. H. Devoret, and R. J. Schoelkopf, Preparation and measurement of three-qubit entanglement in a superconducting circuit, *Nature (London)* **467**, 574 (2010).
- [29] I. Buluta, S. Ashhab, and F. Nori, Natural and artificial atoms for quantum computation, *Rep. Prog. Phys.* **74**, 104401 (2011).
- [30] J. Q. You and F. Nori, Atomic physics and quantum optics using superconducting circuits, *Nature (London)* **474**, 589 (2011).
- [31] E. Lucero, R. Barends, Y. Chen, J. Kelly, M. Mariantoni, A. Megrant, P. O’Malley, D. Sank, A. Vainsencher, J. Wenner, Y. Yin, A. N. Cleland, and J. M. Martinis, Computing prime factors with a Josephson phase qubit quantum processor, *Nat. Phys.* **8**, 719 (2012).
- [32] I. M. Georgescu, S. Ashhab, and F. Nori, Quantum simulation, *Rev. Mod. Phys.* **86**, 153 (2014).
- [33] M. R. Delbecq, V. Schmitt, F. D. Parmentier, N. Roch, J. J. Viennot, G. Fève, B. Huard, C. Mora, A. Cottet, and T. Kontos, Coupling a Quantum Dot, Fermionic Leads, and a Microwave Cavity on a Chip, *Phys. Rev. Lett.* **107**, 256804 (2011).
- [34] J. J. Viennot, J. Palomo, and T. Kontos, Stamping single wall nanotubes for circuit quantum electrodynamics, *Appl. Phys. Lett.* **104**, 113108 (2014).
- [35] V. Ranjan, G. Puebla-Hellmann, M. Jung, T. Hasler, A. Nunnenkamp, M. Muoth, C. Hierold, A. Wallraff, and C. Schönenberger, Clean carbon nanotubes coupled to superconducting impedance-matching circuits, *Nat. Commun.* **6**, 7165 (2015).
- [36] B. H. Schneider, S. Etaki, H. S. J. van der Zant, and G. A. Steele, Coupling carbon nanotube mechanics to a superconducting circuit, *Sci. Rep.* **2**, 599 (2012).
- [37] N. Lambert and F. Nori, Detecting quantum-coherent nanomechanical oscillations using the current-noise spectrum of a double quantum dot, *Phys. Rev. B* **78**, 214302 (2008).
- [38] J. E. Mooij, T. P. Orlando, L. Levitov, L. Tian, C. H. Van der Wal, and S. Lloyd, Josephson persistent-current qubit, *Science* **285**, 1036 (1999).
- [39] J. Q. You, Y. X. Liu, C. P. Sun, and F. Nori, Persistent single-photon production by tunable on-chip micromaser with a superconducting quantum circuit, *Phys. Rev. B* **75**, 104516 (2007).
- [40] J. Q. You, Y.-X. Liu, and F. Nori, Simultaneous Cooling of an Artificial Atom and its Neighboring Quantum System, *Phys. Rev. Lett.* **100**, 047001 (2008).
- [41] A. Fedorov, A. K. Feofanov, P. Macha, P. Forn-Díaz, C. J. P. M. Harmans, and J. E. Mooij, Strong Coupling of a Quantum Oscillator to a Flux Qubit at its Symmetry Point, *Phys. Rev. Lett.* **105**, 060503 (2010).
- [42] M. Stern, G. Catelani, Y. Kubo, C. Grezes, A. Bienfait, D. Vion, D. Esteve, and P. Bertet, Flux Qubits with Long Coherence Times for Hybrid Quantum Circuits, *Phys. Rev. Lett.* **113**, 123601 (2014).

- [43] F. G. Paauw, A. Fedorov, C. J. P. M. Harmans, and J. E. Mooij, Tuning the Gap of a Superconducting Flux Qubit, *Phys. Rev. Lett.* **102**, 090501 (2009).
- [44] X. B. Zhu, A. Kemp, S. Saito, and K. Semba, Coherent operation of a gap-tunable flux qubit, *Appl. Phys. Lett.* **97**, 102503 (2010).
- [45] O. Astafiev, A. M. Zagoskin, A. A. Abdumalikov, Yu. A. Pashkin, T. Yamamoto, K. Inomata, Y. Nakamura, and J. S. Tsai, Resonance fluorescence of a single artificial atom, *Science* **327**, 840 (2010).
- [46] M. J. Schwarz, Gradiometric tunable-gap flux qubits in a circuit QED architecture, Ph.D. thesis, Technische Universität München, München (2015).
- [47] C. M. Wilson, G. Johansson, T. Duty, F. Persson, M. Sandberg, and P. Delsing, Dressed relaxation and dephasing in a strongly driven two-level system, *Phys. Rev. B* **81**, 024520 (2010).
- [48] Y.-X. Liu, C.-X. Yang, H.-C. Sun, and X.-B. Wang, Coexistence of single- and multi-photon processes due to longitudinal couplings between superconducting flux qubits and external fields, *New J. Phys.* **16**, 015031 (2014).
- [49] N. Didier, J. Bourassa, and A. Blais, Fast Quantum Non-demolition Readout by Parametric Modulation of Longitudinal Qubit-Oscillator Interaction, *Phys. Rev. Lett.* **115**, 203601 (2015).
- [50] S. Stenholm, The semiclassical theory of laser cooling, *Rev. Mod. Phys.* **58**, 699 (1986).
- [51] P.-B. Li, Z.-L. Xiang, P. Rabl, and F. Nori, Hybrid Quantum Device with Nitrogen-Vacancy Centers in Diamond Coupled to Carbon Nanotubes, *Phys. Rev. Lett.* **117**, 015502 (2016).
- [52] P. Bertet, I. Chiorescu, G. Burkard, K. Semba, C. J. P. M. Harmans, D. P. DiVincenzo, and J. E. Mooij, Dephasing of a Superconducting Qubit Induced by Photon Noise, *Phys. Rev. Lett.* **95**, 257002 (2005).
- [53] P. Rabl, A. Shnirman, and P. Zoller, Generation of squeezed states of nanomechanical resonators by reservoir engineering, *Phys. Rev. B* **70**, 205304 (2004).
- [54] H.-T. Tan, G.-X. Li, and P. Meystre, Dissipation-driven two-mode mechanical squeezed states in optomechanical systems, *Phys. Rev. A* **87**, 033829 (2013).
- [55] A. Kronwald, F. Marquardt, and A. A. Clerk, Arbitrarily large steady-state bosonic squeezing via dissipation, *Phys. Rev. A* **88**, 063833 (2013).
- [56] X. Wang, H.-R. Li, P.-B. Li, C.-W. Jiang, H. Gao, and F.-L. Li, Preparing ground states and squeezed states of nanomechanical cantilevers by fast dissipation, *Phys. Rev. A* **90**, 013838 (2014).
- [57] J.-M. Pirkkalainen, E. Damskägg, M. Brandt, F. Massel, and M. A. Sillanpää, Squeezing of Quantum Noise of Motion in a Micromechanical Resonator, *Phys. Rev. Lett.* **115**, 243601 (2015).
- [58] F. Marquardt, J. P. Chen, A. A. Clerk, and S. M. Girvin, Quantum Theory of Cavity-Assisted Sideband Cooling of Mechanical Motion, *Phys. Rev. Lett.* **99**, 093902 (2007).
- [59] F. Xue, Y. D. Wang, Y.-X. Liu, and F. Nori, Cooling a micromechanical beam by coupling it to a transmission line, *Phys. Rev. B* **76**, 205302 (2007).
- [60] M. Grajcar, S. Ashhab, J. R. Johansson, and F. Nori, Lower limit on the achievable temperature in resonator-based sideband cooling, *Phys. Rev. B* **78**, 035406 (2008).
- [61] A. Schliesser, R. Rivière, G. Anetsberger, O. Arcizet, and T. J. Kippenberg, Resolved-sideband cooling of a micromechanical oscillator, *Nat. Phys.* **4**, 415 (2008).
- [62] J. D. Teufel, T. Donner, D.-L. Li, J.-W. Harlow, M. S. Allman, K. Cicak, A. J. Sirois, J. D. Whittaker, K. W. Lehnert, and R. W. Simmonds, Sideband cooling of micromechanical motion to the quantum ground state, *Nature (London)* **475**, 359 (2011).
- [63] S. Bose, K. Jacobs, and P. L. Knight, Preparation of nonclassical states in cavities with a moving mirror, *Phys. Rev. A* **56**, 4175 (1997).
- [64] S. Mancini, V. I. Man'ko, and P. Tombesi, Ponderomotive control of quantum macroscopic coherence, *Phys. Rev. A* **55**, 3042 (1997).
- [65] S. Bose, K. Jacobs, and P. L. Knight, Scheme to probe the decoherence of a macroscopic object, *Phys. Rev. A* **59**, 3204 (1999).
- [66] W. Marshall, C. Simon, R. Penrose, and D. Bouwmeester, Towards Quantum Superpositions of a Mirror, *Phys. Rev. Lett.* **91**, 130401 (2003).
- [67] O. Romero-Isart, A. C. Pflanzer, F. Blaser, R. Kaltenbaek, N. Kiesel, M. Aspelmeyer, and J. I. Cirac, Large Quantum Superpositions and Interference of Massive Nanometer-Sized Objects, *Phys. Rev. Lett.* **107**, 020405 (2011).
- [68] B. Pepper, R. Ghobadi, E. Jeffrey, C. Simon, and D. Bouwmeester, Optomechanical Superpositions via Nested Interferometry, *Phys. Rev. Lett.* **109**, 023601 (2012).
- [69] Z.-Q. Yin, T. C. Li, X. Zhang, and L. M. Duan, Large quantum superpositions of a levitated nanodiamond through spin-optomechanical coupling, *Phys. Rev. A* **88**, 033614 (2013).
- [70] S. Nimmrichter and K. Hornberger, Macroscopicity of Mechanical Quantum Superposition States, *Phys. Rev. Lett.* **110**, 160403 (2013).
- [71] J.-Q. Liao and L. Tian, Macroscopic Quantum Superposition in Cavity Optomechanics, *Phys. Rev. Lett.* **116**, 163602 (2016).
- [72] H.-T. Tan, F. Bariani, G.-X. Li, and P. Meystre, Generation of macroscopic quantum superpositions of optomechanical oscillators by dissipation, *Phys. Rev. A* **88**, 023817 (2013).
- [73] M. Asjad and D. Vitali, Reservoir engineering of a mechanical resonator: Generating a macroscopic superposition state and monitoring its decoherence, *J. Phys. B* **47**, 045502 (2014).
- [74] J. D. Thompson, B. M. Zwickl, A. M. Jayich, F. Marquardt, S. M. Girvin, and J. G. E. Harris, Strong dispersive coupling of a high-finesse cavity to a micromechanical membrane, *Nature (London)* **452**, 72 (2008).
- [75] J. C. Sankey, C. Yang, B. M. Zwickl, A. M. Jayich, and J. G. E. Harris, Strong and tunable nonlinear optomechanical coupling in a low-loss system, *Nat. Phys.* **6**, 707 (2010).
- [76] X. Wang, A. Miranowicz, H.-R. Li, and F. Nori, Method for observing robust and tunable phonon blockade in a nanomechanical resonator coupled to a charge qubit, *Phys. Rev. A* **93**, 063861 (2016).
- [77] X. Wang, A. Miranowicz, H.-R. Li, and F. Nori (unpublished).
- [78] M. O. Scully and M. S. Zubairy, *Quantum Optics* (Cambridge University Press, Oxford, 1997).
- [79] A. Kenfack and K. Życzkowski, Negativity of the Wigner function as an indicator of non-classicality, *J. Opt. B* **6**, 396 (2004).
- [80] E. Arimondo, V coherent population trapping in laser spectroscopy, *Prog. Opt.* **35**, 257 (1996).
- [81] M. Fleischhauer, A. Imamoglu, and J. P. Marangos, Electromagnetically induced transparency: Optics in coherent media, *Rev. Mod. Phys.* **77**, 633 (2005).

- [82] P. Anisimov and O. Kocharovskaya, Decaying-dressed-state analysis of a coherently driven three-level Λ system, *J. Mod. Opt.* **55**, 3159 (2008).
- [83] P. M. Anisimov, J. P. Dowling, and B. C. Sanders, Objectively Discerning Autler-Townes Splitting from Electromagnetically Induced Transparency, *Phys. Rev. Lett.* **107**, 163604 (2011).
- [84] B. Peng, S. K. Özdemir, W.-J. Chen, F. Nori, and L. Yang, What is and what is not electromagnetically induced transparency in whispering-gallery microcavities, *Nat. Commun.* **5**, 5082 (2014).
- [85] X. Gu, S.-N. Huai, F. Nori, and Y.-X. Liu, Polariton states in circuit QED for electromagnetically induced transparency, *Phys. Rev. A* **93**, 063827 (2016).
- [86] K. V. R. M. Murali, Z. Dutton, W. D. Oliver, D. S. Crankshaw, and T. P. Orlando, Probing Decoherence with Electromagnetically Induced Transparency in Superconductive Quantum Circuits, *Phys. Rev. Lett.* **93**, 087003 (2004).
- [87] Z. Dutton, K. V. R. M. Murali, W. D. Oliver, and T. P. Orlando, Electromagnetically induced transparency in superconducting quantum circuits: Effects of decoherence, tunneling, and multi-level crosstalk, *Phys. Rev. B* **73**, 104516 (2006).
- [88] X. Wang, H. R. Li, D. X. Chen, W. X. Liu, and F. L. Li, Tunable electromagnetically induced transparency in a composite superconducting system, *Opt. Commun.* **366**, 321 (2016).
- [89] Y.-X. Liu, A. Miranowicz, Y. B. Gao, J. Bajer, C. P. Sun, and F. Nori, Qubit-induced phonon blockade as a signature of quantum behavior in nanomechanical resonators, *Phys. Rev. A* **82**, 032101 (2010).
- [90] A. Miranowicz, J. Bajer, N. Lambert, Y. X. Liu, and F. Nori, Tunable multiphonon blockade in coupled nanomechanical resonators, *Phys. Rev. A* **93**, 013808 (2016).
- [91] A. Miranowicz, R. Tanaś, and S. Kielich, Generation of discrete superpositions of coherent states in the anharmonic oscillator model, *Quantum Opt.: J. Eur. Opt. Soc. B* **2**, 253 (1990).
- [92] A. Miranowicz, M. Paprzycka, A. Pathak, and F. Nori, Phase-space interference of states optically truncated by quantum scissors: Generation of distinct superpositions of qudit coherent states by displacement of vacuum, *Phys. Rev. A* **89**, 033812 (2014).